Data-driven design of metal-organic frameworks for wet flue gas CO_2 capture.

Peter G. Boyd[1*], Arunraj Chidambaram[1*], Enrique García-Díez,[2*] Christopher P. Ireland,[1] Thomas D. Daff[3,4], Richard Bounds[5], Andrzej Gładysiak[1], Pascal Schouwink[6], Seyed Mohamad Moosavi[1], M. Mercedes Maroto-Valer,[2] Jeffrey A. Reimer[5], Jorge A. R. Navarro[7], Tom K. Woo[3†], Susana Garcia,[2†] Kyriakos C. Stylianou,[1†] and Berend Smit[1†]

1. Laboratory of Molecular Simulation (LSMO), Institut des Sciences et Ingénierie Chimiques, Valais (ISIC), École Polytechnique Fédérale de Lausanne (EPFL), Rue de l'Industrie 17, CH-1951 Sion, Switzerland.
2. Research Centre for Carbon Solutions (RCCS), School of Engineering and Physical Sciences, Heriot-Watt University, Edinburgh EH14 4AS, United Kingdom.
3. Department of Chemistry and Biomolecular Science, University of Ottawa, Ottawa, Ontario K1N 6N5, Canada.
4. Current Address: Department of Engineering, Cambridge University, Cambridge, U.K.
5. Department of Chemical and Biomolecular Engineering, University of California, Berkeley 94720, USA.
6. Institut des Sciences et Ingénierie Chimiques (ISIC), École Polytechnique Fédérale de Lausanne (EPFL), CH-1015, Lausanne, Switzerland.
7. Departamento de Química Inorgánica, Universidad de Granada, Av. Fuentenueva S/N, 18071 Granada (Spain).

* These authors contributed equally to this work

† Corresponding Authors: twoo@uottawa.ca, S.Garcia@hw.ac.uk, kyriakos.stylianou@epfl.ch, and berend.smit@epfl.ch

Limiting the increase of CO_2 in our atmosphere is one of the largest challenges of our generation[1]. Because carbon capture and storage is one of the few viable technologies that can mitigate current CO_2 emissions,[2] much effort is focused on developing solid adsorbents that can efficiently capture CO_2 from flue gasses emitted by anthropogenic sources.[3] One class of materials that has attracted much research interest in this context are metal organic frameworks (MOFs), where careful combination of organic ligands with metal-ion nodes can in principle give rise to an innumerable number of structurally and chemically distinct nanoporous MOFs. But an important shortcoming is that many MOFs optimized for CO_2/N_2 separation[4-7] don't perform well when using realistic flue gas containing water,[8] which competes with CO_2 for the same adsorption sites and thereby causes the materials to lose their selectivity. While flue gasses can be dried, this makes the capture process prohibitively expensive.[8,9] Here, we show that data mining of a computational screening library of over 300,000 MOFs can identify different classes of strong CO_2 binding sites (adsorbaphores) that endow MOFs with CO_2/N_2 selectivity persisting in wet flue gasses. We subsequently synthesized two water-stable MOFs containing the most hydrophobic adsorbaphore, finding that their carbon capture performance is indeed not affected by water and outperforms some commercial materials. Further evaluation will require testing of performance in an industrial setting, and considering the full capture process (including the targeted CO_2 sink, such as geological storage or serving as carbon source for the chemical industry) to identify the optimal separation material.

Different strategies have been developed to mitigate the negative effects of water on the CO_2/N_2 separation selectivity in MOF materials. For example, for MOFs with open metal sites, these sites can be used to attach amines, taking advantage of the specific amine chemistry that is also used in conventional amine scrubbing.[10-13] Chanut *et al.* [14] carried out a screening study to investigate whether MOFs, as such, can adsorb CO_2 in the presence of water. Their screening study hints that such MOFs could be de novo designed. In this work, we develop a systematic strategy to tailor make MOFs that can capture carbon from wet flue gasses. Our design methodology is inspired by the rational design of drug molecules, wherein organic molecules that fit well into the binding pocket of a protein are mined from databases of known chemicals.[15,16] The difference is that in our case the "drug molecule" is known (i.e., CO_2), but not the substrate that binds it optimally (i.e., the MOF). Hence, we generated a library of 325,000 hypothetical MOFs, and screened each material for its CO_2/N_2 selectivity and CO_2 working capacity. The chemical building blocks used in the generation of these materials are sketched in Extended Data Figs. 1 and 2. Fig. 1a shows that 8,325 hypothetical materials possess a working capacity for CO_2 greater than 2 mmol/g and a CO_2/N_2 selectivity greater than 50, surpassing the performance of zeolite 13x under dry conditions.[17]

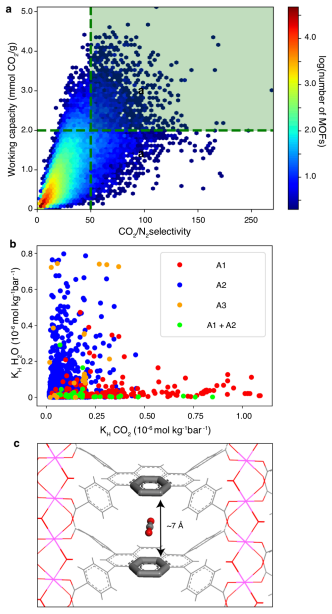

Fig. 1 | Computational screening of MOFs for strong CO_2 adsorption and selectivity. a, the results from the screening of 325,000 hypothetical MOFs at conditions that mimic post-combustion capture (adsorption at ambient temperature and 1 bar with a molar ratio of 15:85 CO_2/N_2 and regeneration at 363 K and 0.1 bar). The materials in the green box were selected for more refined screening and adsorbaphore identification; the color-coding represents the number of MOFs. **b**, The H_2O affinity of the top performing materials as characterized by the H_2O vs CO_2 Henry coefficients. The color codes represent the three different adsorbaphores found in the top performing structures; A1 – parallel aromatic rings, A2 – metal-oxygen bridges, and A3 – open metal sites. Some materials have both A1 and A2 sites. **c**, The parallel aromatic rings adsorbaphore discovered with the feature recognition algorithm.

A key component in drug design is to analyze the optimally binding molecules for a common feature or spatial arrangement of atoms of the binding site, which is referred to as the pharmacophore.[15] Analogously, we coin the term

adsorbaphore to describe the common pore shape and chemistry of a binding site in a MOF that provides optimal interactions to preferentially bind to a particular guest molecule, in this case CO_2. From our top ranked 8,325 materials we identified 106,680 such CO_2 binding sites (see Extended Data Fig. 3 for some examples). A similarity analysis of these binding sites resulted in three main classes of adsorbaphore being observed: A1) two parallel aromatic rings with interatomic spacing of approximately 7Å (31% of all binding sites), A2) metal–oxygen–metal bridges (32%), and A3) open metal sites (21%), see SI for details. Subsequently, we screened the materials possessing these adsorbaphores for their affinity for water. Fig. 1b shows the Henry coefficient for water in these high performing materials. Analysis of the data shows that the materials with the parallel aromatic rings adsorbaphore (A1) have a low Henry coefficient for H_2O, while the metal-oxygen bridges (A2) and open metal sites (A3) tend to have higher Henry coefficients (Fig. 1b). A graphical representation of the different adsorbaphores is presented in Extended Data Fig 4. Indeed, comparison of the binding energies, computed at the DFT level, for the adsorbaphore shown in Fig. 1c, indicates a preference for CO_2 (-10.2 kcal/mol) over N_2 and H_2O by 2.7 and 1.5 kcal/mol, respectively (see Extended Data Table 1). The parallel aromatic rings provide a near optimum interaction with all three atoms of CO_2, while for H_2O the lack of hydrogen bonding sites limits its binding energy.

The next step is to identify a subclass of MOFs in our library that contains the preferred adsorbaphore. From an experimental point of view, MOFs with the **frz** topology, characterized by tetra-carboxylated organic ligands coordinated to 1D metal – oxygen rods are an attractive starting point. One of these has been synthesized with indium as a metal node giving a structurally stable, non-breathing MOF.[18] In this topology, the metal rods provide an ideal scaffolding to which we can attach our adsorbaphore. By choosing the metal ion we have some flexibility to tune the distance between the aromatic rings. Our calculations predict that if we replace In(III) by Al(III) we approach the ideal adsorbaphore distance of 6.5 – 7.0 Å (see Extended Data Table 2) which was determined by adjusting the spacing of the aromatic rings incrementally (Extended Data Fig. 5). In addition, aluminum is an attractive choice as it is an abundant metal and it ensures a strong bond with the carboxylate O-atoms of the ligands,[19] which significantly improves the thermal and hydrolytic stability of a MOF.[20,21]

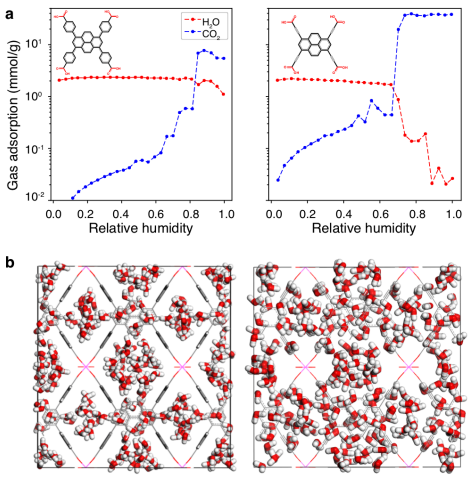

Fig. 2 | **Effects of water on different MOFs with the same adsorbaphore. a,** and **b,** Simulated adsorption of a ternary mixture of $CO_2/N_2/H_2O$ at 313 K. The partial pressure of CO_2 is held at 0.15 bar while the relative humidity increases. The N_2 uptake was negligible and not shown. **c,** and **d,** Visualization of the water loading at 100% relative humidity in (**c**) hypothetical MOF **m8o67** and **d**, hypothetical MOF **m8o71**. The benzoate groups are represented by grey sticks and water by red and white space filling atoms. Note that in **m8o67** the benzoate groups perpendicular to the plane of the figure prevent H-bond formation across the adsorbaphores.

Using our MOF generation algorithm[22], we generated a library of 35 isoreticular materials and computed from the mixture isotherms the CO_2/N_2 selectivity in dry and wet flue gasses (Extended Data Figs. 6 and 7). Our calculations show that all our predicted materials maintain an excellent selectivity at low pressures, and in approximately 75% of these materials, the selectivity was not influenced by the presence of water at flue gas conditions. The concept of an adsorbaphore focusses on the design of an adsorption site that optimizes selectivities at low pressure. At higher partial water pressure, water adsorption is dominated by the energetics of hydrogen bond formation. Further analyses showed that the pore shape of the materials that maintain a high CO_2

uptake at high humidity frustrates the formation of these hydrogen bonds. This is illustrated in Figs. 2a,b which compares the water impact on the CO_2 uptake of two materials with the same adsorbaphore but different pore structures (hypothetical MOFs **m8o67** and **m8o71**). Fig. 2a show that **m8o67** is resistant to H_2O flooding; even at a relative humidity of approximately 85% we only see a small effect of H_2O on CO_2 capacity. Conversely, **m8o71** completely loses its CO_2 capacity at 60% relative humidity (Fig. 2b). In Figs. 2c,d we visualize the H-bond network that is formed at 100% relative humidity in both materials. For material **m8o71**, we see a complete H-bond network (Fig. 2d), while for **m8o67** (Fig. 2c) we observe a less extensive network; the benzoate groups separating the adsorbaphores frustrate the formation of a complete H-bonding network.

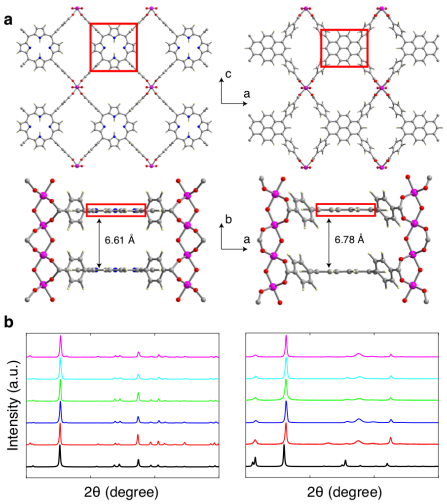

Fig. 3 | Structural representation and stability of [Al-PMOF] and [Al-PyrMOF]. a, and **b,** Ball and stick representation of the **[Al-PMOF]** and **[Al-PyrMOF]** structures, respectively. The orientation of the tetra-carboxylate ligands around the Al(III) rods results in the generation of the 3D-non interpenetrated structures containing the adsorbaphore (red box). Atom color code: pink: Al; grey: C; blue: N; red: O and pale yellow: H. **c,** and **d,** laboratory PXRD patterns of **[Al-PMOF]** and **[Al-PyrMOF]**, respectively – black, simulated; red, as made; blue, acetone exchanged; green, activated; sky blue, activated material immersed in liquid water for 7 days, and pink, exposed in controlled vapor atmosphere of nitric acid for 3 hours.

On the basis of these predictions, we synthesized two **frz**-based MOFs using organic ligands that possess the water-frustrating properties reported above: **Al-PMOF**[19] (**m8o66**) and **Al-PyrMOF (m8o67).** These MOFs are based on Al(III) 1-dimensional rods linked by the TCPP (tetrakis-(4-carboxyphenyl)-porphyrin), and TBAPy (1,3,6,8-tetrakis-(*p*-benzoic acid)-pyrene) ligands, respectively (Figs. 3a,b). Fig. 3c,d show no loss of their crystallinity upon activation, as well as exposure to different harsh conditions, including immersion in water for 7 days. Further characterization of both materials (see SI) shows excellent agreement with the predicted cell parameters.

By discovering the existence of adsorbaphores in these hypothetical materials, we assume that our *in silico* screening method can correctly predict 1) the structure of a MOF, 2) the adsorption properties, and 3) the nature of the binding sites of CO_2 and H_2O. With **Al-PMOF** and **Al-PyrMOF**, we can test these assumptions. In Fig. 4a, we show that the experimental and predicted CO_2 and N_2 adsorption isotherms are in good agreement. The CO_2 binding positions in the adsorbaphore, and the impact of H_2O are more challenging to observe experimentally. The siting of CO_2 was studied using *in-situ* CO_2 loading powder X-ray diffraction. Upon loading, we observed a significant change in the intensity and peak position of the Bragg reflections (see Fig. S2.1). Subsequent Rietveld refinement and Fourier analysis[23] provided us with the preferred locations of CO_2 in the pores of **Al-PMOF** shown in Fig. 4b. These results confirm that CO_2 preferentially adsorbs in the adsorbaphore.

The effect of water on the siting of CO_2 has been further addressed with solid-state NMR. Under conditions of magic angle spinning, high resolution ^{13}C NMR chemical shifts are very sensitive to changes in the chemical environment. The ^{13}C NMR spectra of **Al-PyrMOF** and **Al-PMOF** are shown in the Extended Data Fig. 8 where we also assign these peaks to specific atoms on the MOF. The chemical shifts associated with the atoms of the adsorbophore (see inset) are shown in Fig. 4c as a function of the water concentration. At low water loadings the adsorbophore atoms experience no change in chemical environment with water loading, and at the highest water loadings there are modest changes in the carbon-13 chemical shifts of only those atoms proximate to the

aluminium-coordinated carboxylate groups next to the adsorbaphore (carbons B and F in Fig. 4c). This broadening is consistent with dipolar broadening from proximate water molecules, thus confirming that the adsorbaphore itself is not a preferential adsorption site for H_2O.

Our simulations predict that CO_2 adsorbed in the adsorbaphore is insulated from adsorption of water. As the ^{13}C NMR spectrum of adsorbed $^{13}CO_2$ is extremely sensitive to the proximity of water molecules via its chemical shift and line broadening, any disruption of the chemical environment of adsorbed CO_2 by water should be immediately apparent. Fig. 4d shows that the chemical shift of the adsorbed $^{13}CO_2$ is independent of water content. However, we do see a broadening of the ^{13}C NMR line with increasing humidity. If this broadening is due to the proximity of the protons in water, it should disappear if we repeat the experiments with D_2O. Fig. 4d shows it does not. This nicely confirms our simulation results, shown in Fig. 2c, on the limited effect of water on CO_2 adsorption in **Al-PyrMOF**.

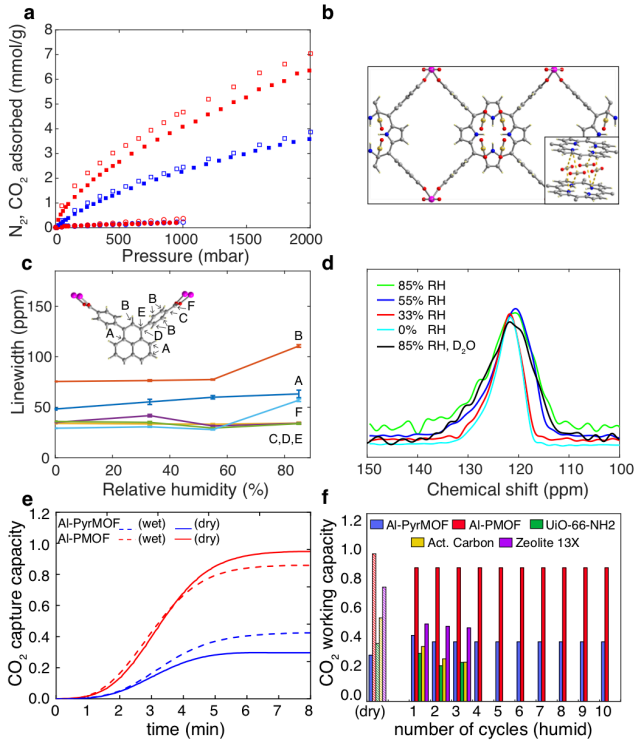

Fig. 4 | CO_2 adsorption, ^{13}C CP-NMR, and breakthrough experiments for [Al-PMOF] and [Al-PyrMOF]. **a**, comparison of experimental (filled) and computational (open) single component adsorption isotherms for CO_2 (squares) and N_2 (circles) adsorption collected on activated [Al-PMOF] (red) and [Al-PyrMOF] (blue) at 313 K. **b**, Rietveld refinement of the XRD data shown in SI revealed that CO_2 binding in [Al-PMOF] occurs between the porphyrin cores – the adsorbaphore, **c**, ^{13}C CP-MAS spectrum of [Al-PyrMOF] recorded as a function of relative humidity: linewidth change for each C of the TBAPy ligand. The inset provides labels for each carbon atom in the ligand, **d**, Linewidth vs relative humidity (H_2O) extracted from ^{13}C static spectra of $^{13}CO_2$ loaded in [Al-PyrMOF]. **e**, CO_2 capture capacity profiles (in mmol/g) for [Al-PyrMOF] and [Al-PMOF] during breakthrough experiments under dry and humid (85%RH) conditions, with 85/15 v/v of N_2/CO_2 (313 K and 1 bar). **f,** Benchmarking of CO_2 working capacity (in mmol/g) for [Al-PyrMOF] and [Al-PMOF] versus UiO-66-NH2, activated carbon, and zeolite 13X under dry and humid (85%RH) conditions, with 85/15 v/v of N_2/CO_2 (313 K and 1 bar). For wet flue gasses we studied the performance stability after 3 cycles for reference materials, and after 10 cycles for [Al-PyrMOF] and [Al-PMOF].

An important practical test is to evaluate whether these materials can capture CO_2 from wet flue gases. Hence, we determined the capture capacity using a breakthrough experiment for both **Al-PMOF** and **Al-PyrMOF** of a mixture of CO_2/N_2 under dry- and humid-conditions (Fig. 4e).[24] These results confirm the predictions of the simulations (Extended Data Fig. 7) that for **Al-PMOF** the capture capacity is minimally influenced by humidity in the flue gasses, while for **Al-PyrMOF** we even observe an enhancement of the performance. Furthermore, repeated cycling[25] (Fig. 4f) does not show a degradation of the material nor that their separation performance is changed. It is instructive to compare the performance of our materials with a set of reference materials, which include commercially available ones, such as, zeolite 13X and activated carbon, and a water stable, amino-functionalized MOF, UiO-66-NH2. For dry flue gasses these materials have a capture capacity between **Al-PyrMOF** and **Al-PMOF**, but unlike our MOFs in humid flue gasses the performance reduces significantly. Our materials are not the ones with the highest working capacity,[14] yet it is encouraging to see that in wet flue gasses **Al-PMOF** outperforms commercial materials, like, zeolite 13X and activated carbon.

Although the large-scale screenings of databases of hypothetical MOFs have been previously reported for various gas separation and storage applications,[26-29] the synthesis of new materials identified as high performing from those screenings is lacking. In this work, we have developed a data-driven method to identify binding pockets or structural motifs called adsorbaphores; these motifs are targeted for synthesis rather than a whole material. This enhances the synthetic viability of the approach as demonstrated by the fact that one material with the targeted adsorbaphore, which has not previously been reported, was synthesized and shown to adsorb CO_2 as predicted. The concept of linking the computational screening and synthesis of the materials through the adsorbaphores should be applicable to other gas separations of increasing complexity.

REFERENCES AND NOTES

1 Smit, B., Reimer, J. R., Oldenburg, C. M. & Bourg, I. C. *Introduction to Carbon Capture and Sequestration*. (Imperial College Press, 2014).

2 Bui, M. *et al.* Carbon capture and storage (CCS): the way forward. *Energ Environ Sci* **11**, 1062-1176, doi:10.1039/c7ee02342a (2018).

3 D'Alessandro, D. M., Smit, B. & Long, J. R. Carbon Dioxide Capture: Prospects for New Materials. *Angew. Chem.-Int. Edit.* **49**, 6058-6082, doi:10.1002/anie.201000431 (2010).

4 Sumida, K. *et al.* Carbon Dioxide Capture in Metal-Organic Frameworks. *Chemical Reviews* **112**, 724-781, doi:10.1021/cr2003272 (2012).

5 Furukawa, H., Cordova, K. E., O'Keeffe, M. & Yaghi, O. M. The Chemistry and Applications of Metal-Organic Frameworks. *Science* **341**, 974, doi:10.1126/Science.1230444 (2013).

6 Huck, J. M. *et al.* Evaluating different classes of porous materials for carbon capture. *Energ Environ Sci* **7**, 4136-4146, doi:10.1039/C4EE02636E (2014).

7 Mason, J. A., Sumida, K., Herm, Z. R., Krishna, R. & Long, J. R. Evaluating metal-organic frameworks for post-combustion carbon dioxide capture via temperature swing adsorption. *Energ Environ Sci* **4**, 3030-3040, doi:10.1039/c1ee01720a (2011).

8 Li, G. *et al.* Capture of CO2 from high humidity flue gas by vacuum swing adsorption with zeolite 13X. *Adsorption-Journal of the International Adsorption Society* **14**, 415-422, doi:10.1007/s10450-007-9100-y (2008).

9 Merel, J., Clausse, M. & Meunier, F. Experimental investigation on CO2 post-combustion capture by indirect thermal swing adsorption using 13X and 5A zeolites. *Industrial & Engineering Chemistry Research* **47**, 209-215, doi:10.1021/ie071012x (2008).

10 Milner, P. J. *et al.* A Diaminopropane-Appended Metal-Organic Framework Enabling Efficient CO2 Capture from Coal Flue Gas via a Mixed Adsorption Mechanism. *J. Am. Chem. Soc.* **139**, 13541-13553, doi:10.1021/jacs.7b07612 (2017).

11 McDonald, T. M. *et al.* Cooperative insertion of CO2 in diamine-appended metal-organic frameworks. *Nature* **519**, 303-308, doi:10.1038/nature14327 (2015).

12 Faig, R. W. *et al.* The Chemistry of CO2 Capture in an Amine-Functionalized Metal-Organic Framework under Dry and Humid Conditions. *J. Am. Chem. Soc.* **139**, 12125-12128, doi:10.1021/jacs.7b06382 (2017).

13 Couck, S. *et al.* An Amine-Functionalized MIL-53 Metal-Organic Framework with Large Separation Power for CO2 and CH4. *J. Am. Chem. Soc.* **131**, 6326-+, doi:10.1021/ja900555r (2009).

14 Chanut, N. *et al.* Screening the Effect of Water Vapour on Gas Adsorption Performance: Application to CO2 Capture from Flue Gas in Metal-Organic Frameworks. *ChemSusChem* **10**, 1543-1553, doi:10.1002/cssc.201601816 (2017).

15 Wolber, G., Seidel, T., Bendix, F. & Langer, T. Molecule-pharmacophore superpositioning and pattern matching in computational drug design. *Drug Discov Today* **13**, 23-29, doi:10.1016/j.drudis.2007.09.007 (2008).

16 Sliwoski, G., Kothiwale, S., Meiler, J. & Lowe, E. W. Computational Methods in Drug Discovery. *Pharmacol Rev* **66**, 334-395, doi:10.1124/pr.112.007336 (2014).
17 Ho, M. T., Allinson, G. W. & Wiley, D. E. Reducing the cost of CO2 capture from flue gases using pressure swing adsorption. *Industrial & Engineering Chemistry Research* **47**, 4883-4890, doi:10.1021/ie070831e (2008).
18 Stylianou, K. C. *et al.* A Guest-Responsive Fluorescent 3D Microporous Metal-Organic Framework Derived from a Long-Lifetime Pyrene Core. *J. Am. Chem. Soc.* **132**, 4119-4130, doi:10.1021/ja906041f (2010).
19 Fateeva, A. *et al.* A Water-Stable Porphyrin-Based Metal-Organic Framework Active for Visible-Light Photocatalysis. *Angew. Chem.-Int. Edit.* **51**, 7440-7444, doi:10.1002/anie.201202471 (2012).
20 Loiseau, T. *et al.* A rationale for the large breathing of the porous aluminum terephthalate (MIL-53) upon hydration. *Chem.-Eur. J.* **10**, 1373-1382, doi:10.1002/chem.200305413 (2004).
21 Reinsch, H. & Stock, N. High-throughput studies of highly porous Al-based MOFs. *Microporous Mesoporous Mat.* **171**, 156-165, doi:10.1016/j.micromeso.2012.12.024 (2013).
22 Boyd, P. G. & Woo, T. K. A generalized method for constructing hypothetical nanoporous materials of any net topology from graph theory. *Crystengcomm* **18**, 3777-3792, doi:10.1039/c6ce00407e (2016).
23 Carrington, E. J., Vitorica-Yrezabal, I. J. & Brammer, L. Crystallographic studies of gas sorption in metal-organic frameworks. *Acta Crystallographica Section B-Structural Science Crystal Engineering and Materials* **70**, 404-422, doi:10.1107/S2052520614009834 (2014).
24 Garcia, S. *et al.* Breakthrough adsorption study of a commercial activated carbon for pre-combustion CO2 capture. *Chemical Engineering Journal* **171**, 549-556, doi:10.1016/j.cej.2011.04.027 (2011).
25 Garcia, S., Gil, M. V., Pis, J. J., Rubiera, F. & Pevida, C. Cyclic operation of a fixed-bed pressure and temperature swing process for CO2 capture: Experimental and statistical analysis. *Int. J. Greenh. Gas Control* **12**, 35-43, doi:10.1016/j.ijggc.2012.10.018 (2013).
26 Lin, L.-C. *et al.* In silico screening of carbon-capture materials. *Nat. Mater.* **11**, 633-641, doi:10.1038/nmat3336 (2012).
27 Wilmer, C. E. *et al.* Large-scale screening of hypothetical metal organic frameworks. *Nat Chem* **4**, 83-89, doi:10.1038/nchem.1192 (2012).
28 Boyd, P. G., Lee, Y. & Smit, B. Computational development of the nanoporous materials genome. *Nature Materials Review* **2**, 17037, doi:10.1038/natrevmats.2017.37 (2017).
29 Yazaydin, A. O. *et al.* Screening of Metal-Organic Frameworks for Carbon Dioxide Capture from Flue Gas Using a Combined Experimental and Modeling Approach. *J. Am. Chem. Soc.* **131**, 18198-+, doi:10.1021/ja9057234 (2009).

Supplementary Information is available in the online version of the paper**.**

Acknowledgments

S.G., J.A.R, and B.S. acknowledge support during the final stage of the work of the ACT PriSMa project, which has received funding from BEIS (UK), DOE Office of Fossil Energy (USA), and Office Fédéral de l'Energie (Switzerland). K.C.S. is supported by the Swiss National Science Foundation (SNF) under the Ambizione Energy Grant n.PZENP2_166888, P.G.B. and B.S. by the European Research Council (ERC) Advanced Grant (Grant Agreement No. 666983, MaGic) and the National Center of Competence in Research (NCCR), Materials' Revolution: Computational Design and Discovery of Novel Materials (MARVEL). A.C. C.P.I., and S.M.M. were supported by European Union's Horizon 2020 research and innovation programme under grant agreement No 760899 (GENESIS). R.B. and J.A.R. were supported by the Center for Gas Separations Relevant to Clean Energy

Technologies, an Energy Frontier Research Center funded by the DOE, Office of Science, Office of Basic Energy Sciences under award DE-SC0001015. E.G. is supported by the European Commission under the Research Fund for Coal and Steel (RFCS) Programme (Project No 709741). M.M.V and S.G. acknowledge the financial support from the Engineering and Physical Sciences Research Council (EP/N024540/1) and the Research Centre for Carbon Solutions (RCCS) at Heriot-Watt University. The authors thank the Swiss Norwegian Beamlines of ESRF for beamtime allocation at BM31 for the in-situ CO_2 loading and variable temperature PXRD experiments. This work was supported by a grant from the Swiss National Supercomputing Center (CSCS) under Project no. s761, as well as resources from the National Energy Research Scientific Computing Center, a DOE Office of Science User Facility supported by the Office of Science of the U.S. Department of Energy under the Contract No. DE-AC02-05CH11231. JARN thanks Spanish MINECO (CTQ2017-84692-R) and EU Feder funding. S.G. and B.S. would like to acknowledge the support of Mission Innovation Carbon Capture Challenge Initiative.

Author Contributions P.G.B., T.K.W., and B.S. developed the MOF generation algorithm, the adsorbaphore identification and analysis, and Monte Carlo simulations, T.D.D. carried out the initial computational screening. S.M.M. carried out the similarity analysis, A.C., C.P.I., and K.C.S. synthesized and characterized the materials. The breakthrough experiments were carried out by E.G., C.P.I., A.C., M.M., J.A.R.N, and S.G. The NMR experiments were carried out by R.B. and J.A.R. The X-ray analysis was carried out by A.G. and P.S. All authors contributed to the analysis of the data and the writing of the article.

Competing interests K.C.S., B.S., A.C., P.G.B., and T.K.W. have filed a patent application (No. 18 168 544.7) that relates to water stable polyaromatic MOF materials for CO_2 separation from flue gas and natural gas streams.

Author Information Reprint and permission information is available at www.nature.com/reprints. The authors declare competing financial interests: details are available in the online version of the paper. Readers are welcome to comment on the online version of the paper. Correspondence and requests for materials should be addressed to T.K.W. (twoo@uottawa.ca), S.G. (S.Garcia@hw.ac.uk), K.C.S. (kyriakos.stylianou@epfl.ch), or B.S. (berend.smit@epfl.ch).

Data Availability The computed data and hypothetical materials that were used in this publication are provided free of charge on the Materials Cloud (DOI: 10.24435/materialscloud:2018.0016/v1). On this site one can also find an interactive version of Figs. 1 a and b. Data that are not included in the paper are available upon reasonable request to the authors.

Code Availability. Topology Based Crystal Constructor (ToBasCCo), the python program used to build hypothetical MOFs is hosted on GitHub https://github.com/peteboyd/tobascco. The python code that compares common chemical features between fragments is provided on GitHub: https://github.com/peteboyd/adsorbaphore and is dependent on a C library called MCQD which performs the maximum clique detection of the chemical graphs. An interface between python and C for this is provided here: https://github.com/peteboyd/mcqd_api. The Automatic Binding Site Locator (ABSL) program, used to identify CO_2 binding sites in each MOF, is part of a broader python-based code used to facilitate simulations of porous materials called Fully Automated Adsorption Analysis in Porous Solids (FA^3PS). This is available on BitBucket: https://bitbucket.org/tdaff/automation.

EXTENDED DATA

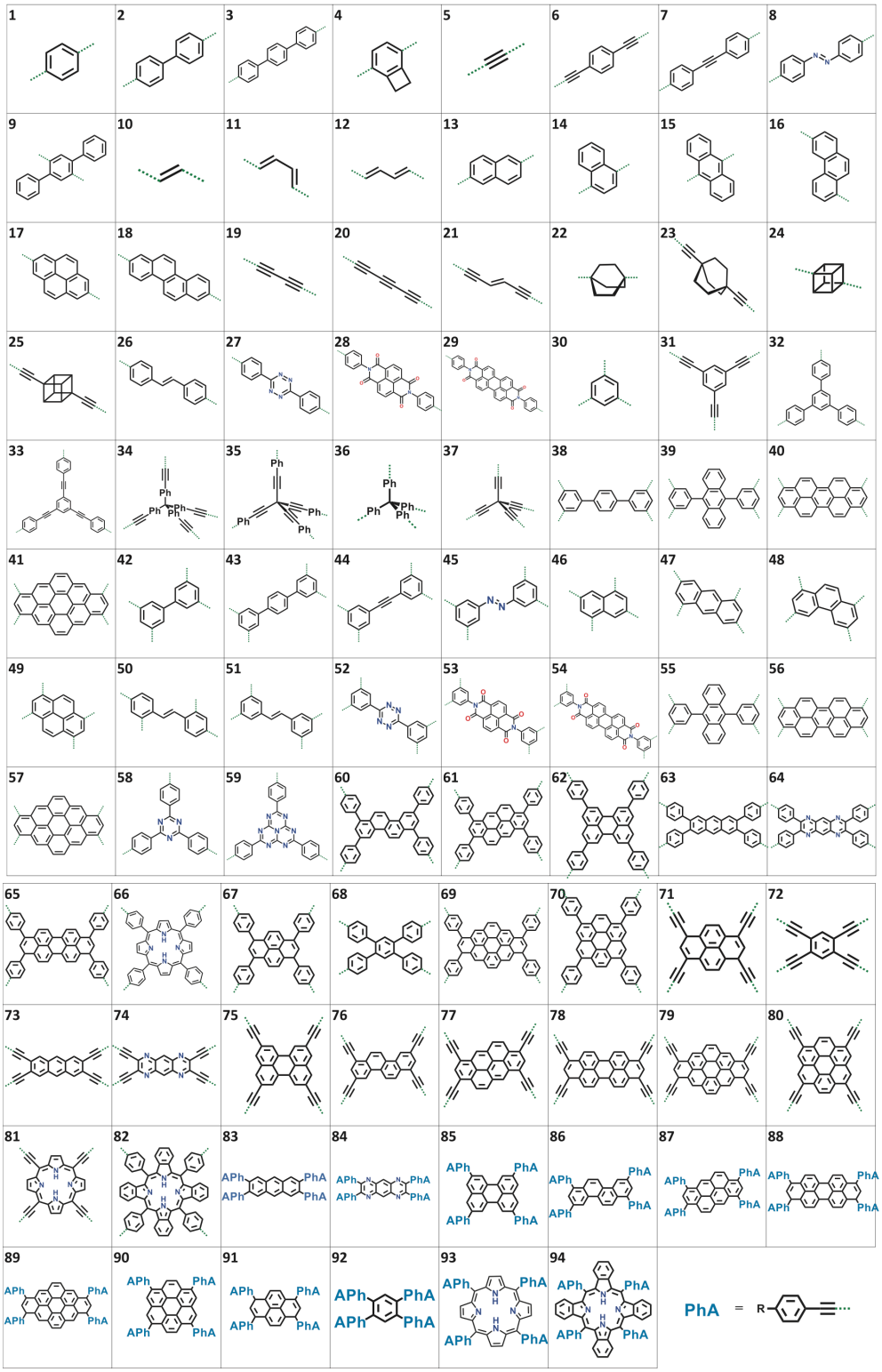

Extended Data Figure 1 | **Hypothetical material generation (1).** The organic Secondary Building Units (SBUs) used in the generation of the hypothetical MOF database.

a

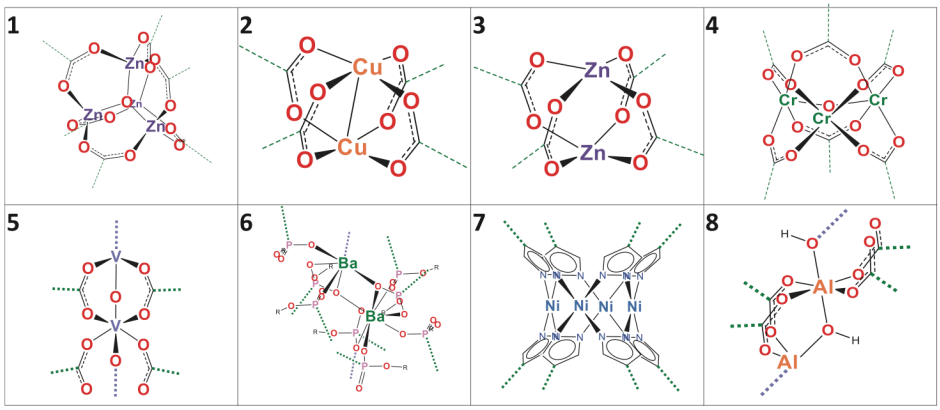

b

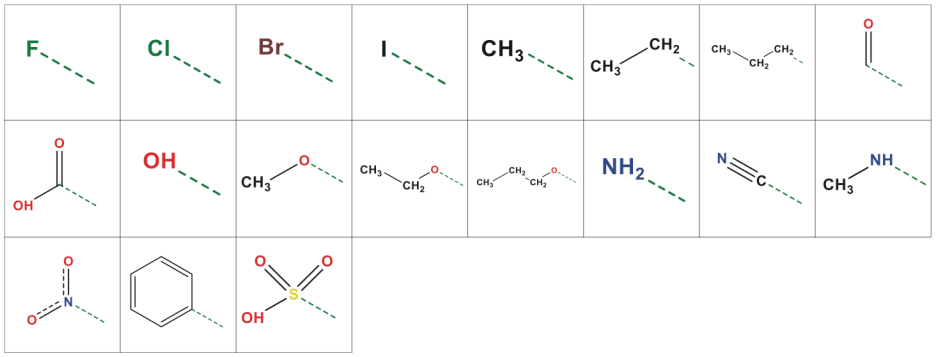

Extended Data Figure 2 | Hypothetical material generation (2). a, Metal SBUs used in the generation of the hypothetical MOF database. **b**, functional groups used to decorate the unfunctionalized hypothetical MOFs in the database. We denote a hypothetical material by **mXoYY**, where X refers to the metal SBU shown in the Extended Data Figure 2(a) and YY to the organic SBU shown in Extended Data Figure 1. Functional groups were decorated on the base hypothetical materials using an internal numbering system. The data is available online at [DOI: 10.24435/materialscloud:2018.0016/v1].

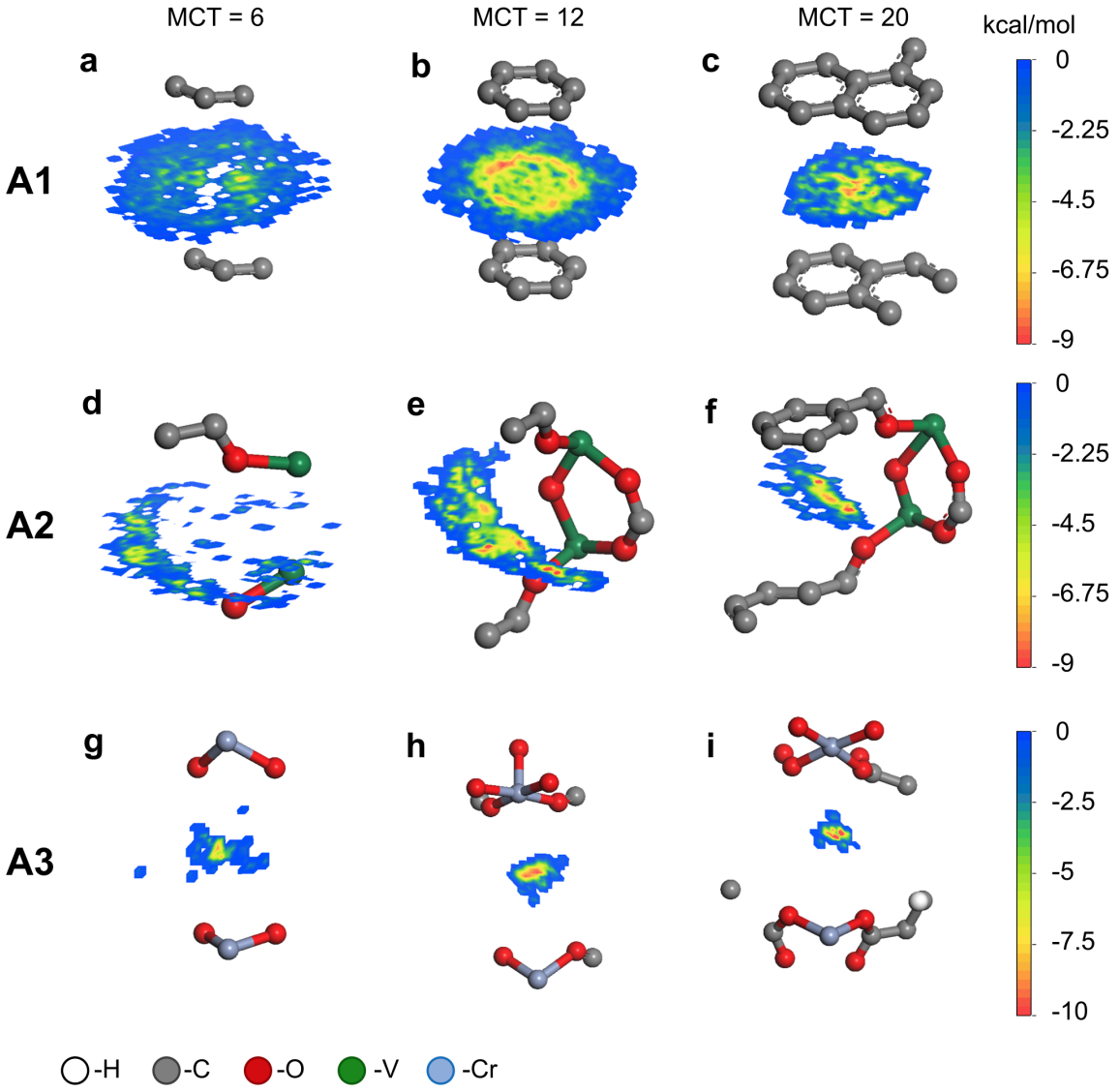

Extended Data Figure 3 | Examples of Adsorbaphores. A selection of the most representative adsorbaphores found from visual inspection of the top 50 most frequent adsorbaphores found from the random pairing method described in the SI. There are three major trends in the molecular fragments which can be seen going down the columns of the image, labelled A1, A2 and A3. The chemical features of the fragments increase as one goes across each row. This is accomplished by increasing the minimum number of common atoms allowed during the substructure search, called the Minimum Clique Threshold (MCT). Pictured in each adsorbaphore is a representative contour map of the energy produced from CO_2 binding with the adsorbaphore atoms from each original CO_2 binding site. **a-c**, **A1**: planar aromatic systems where CO_2 binds in between, **d-f**, **A2**: CO_2 binding near the bridging oxygen of a pillared vanadium SBU, **g-I**, **A3**: CO_2 bound between open-metal Cr SBUs.

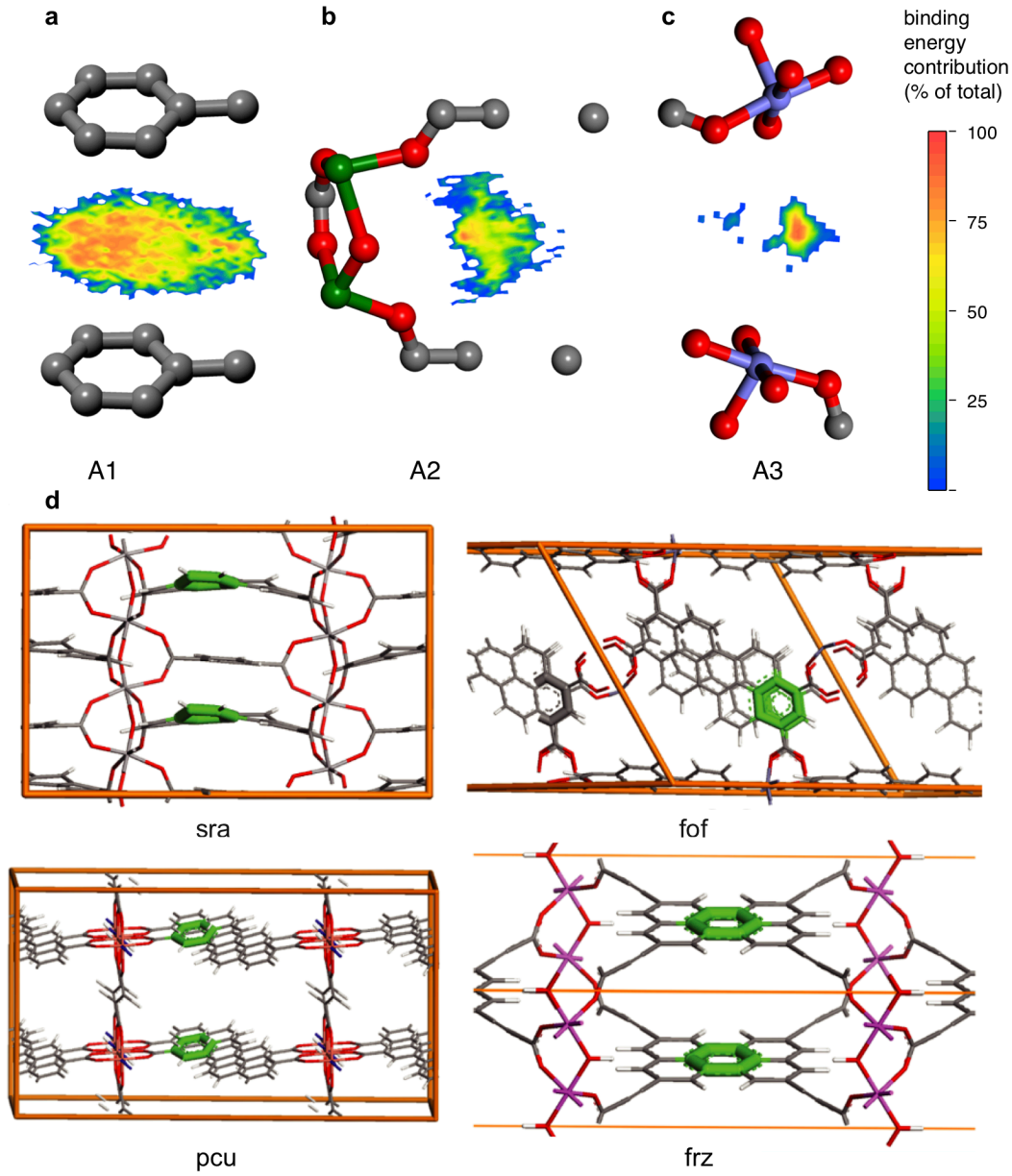

Extended Data Figure 4| Commonly found adsorbaphores. a-c, commonly found adsorbaphores from the maximum clique detection method. Atom colors: grey – carbon, red – oxygen, green – vanadium, blue – chromium. **d**, Representative adsorbaphore **A1** found in different hypothetical MOFs from the hypothetical database. The adsorbaphore atoms are highlighted green.

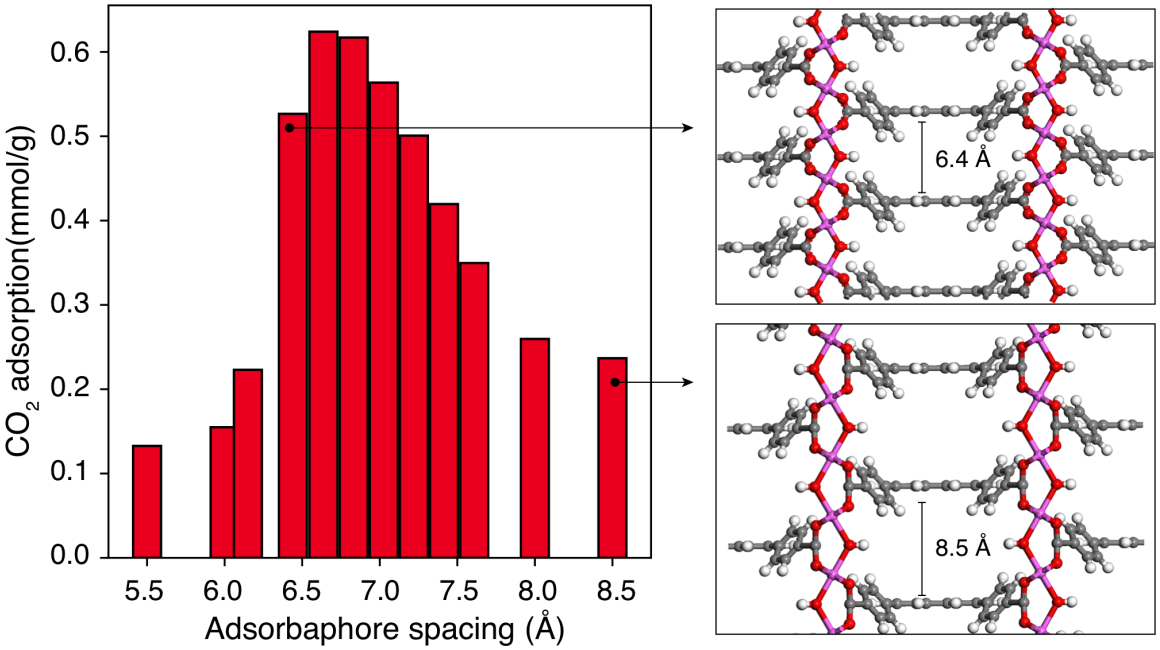

Extended Data Figure 5 | **Effect of the adsorbaphore spacer. a**, plot of the CO_2 adsorption at 0.15 bar, 313K in hypothetical MOFs consisting of the **frz** topology, metal node #8 and organic linker #67 (m8o67). The interplanar spacing of the adsorbaphore atoms is adjusted re-assembling the structure with larger or smaller Al-O bonds. **b,** graphical representation of the spacing adjustments made to the material.

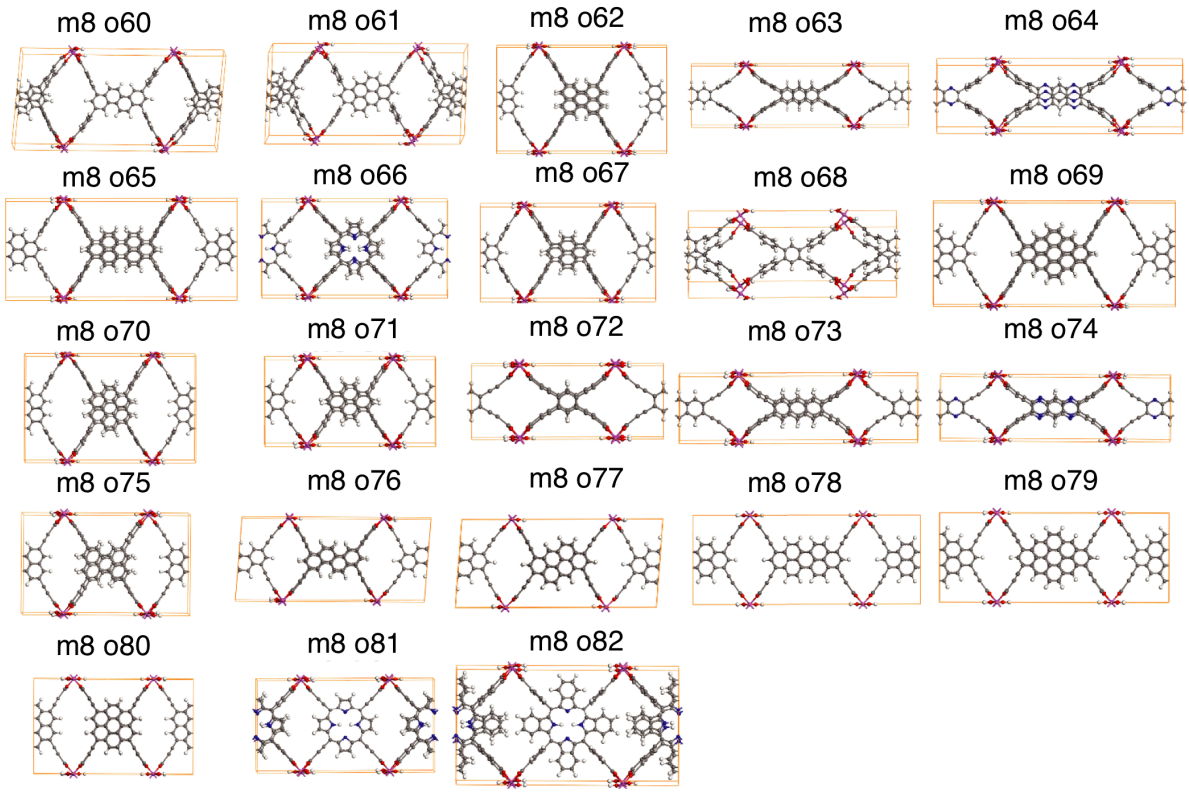

Extended Data Figure 6 | Hypothetical MOFs built with the frz topology. These structures contain an Al 1D rod (m8) and the organic ligands 60-82 from Figs. S1 and S2. The spacing between parallel aromatic cores (seen in the centre of each hypothetical MOF) is ~6.7 Å, defining the adsorbaphore site in each material. No functional groups were used to decorate these materials. We refer to synthesized version of m8o66 and m8o67 as **Al-PMOF** (**$Al_2(OH)_2(H_2TCPP)$**) and **AlPyrMOF** (**$Al_2(OH)_2(TBAPy)$**), respectively.

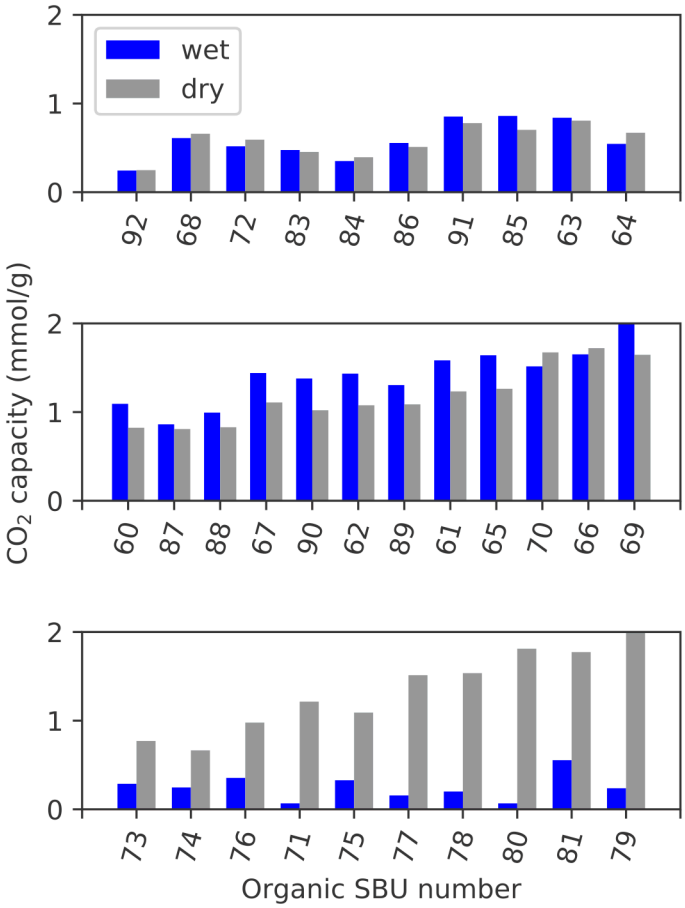

Extended Data Figure 7 | CO_2 adsorption capacity of a class of frz-based hypothetical MOFs at 0.15 bar and 313K under 'wet' (85% RH) and 'dry' flue gas conditions. a-b, where the organic ligand is connected to the Al metal ion via 4 benzoate moieties and **c**, where the organic ligand is connected to the Al metal ion via 4 acetylenic carboxylate moieties. The materials are ranked from lowest adsorbaphore density to highest, and number YY on the x-axis correspond to the organic linker number in m8oYY (see Extended Data Fig. 6).

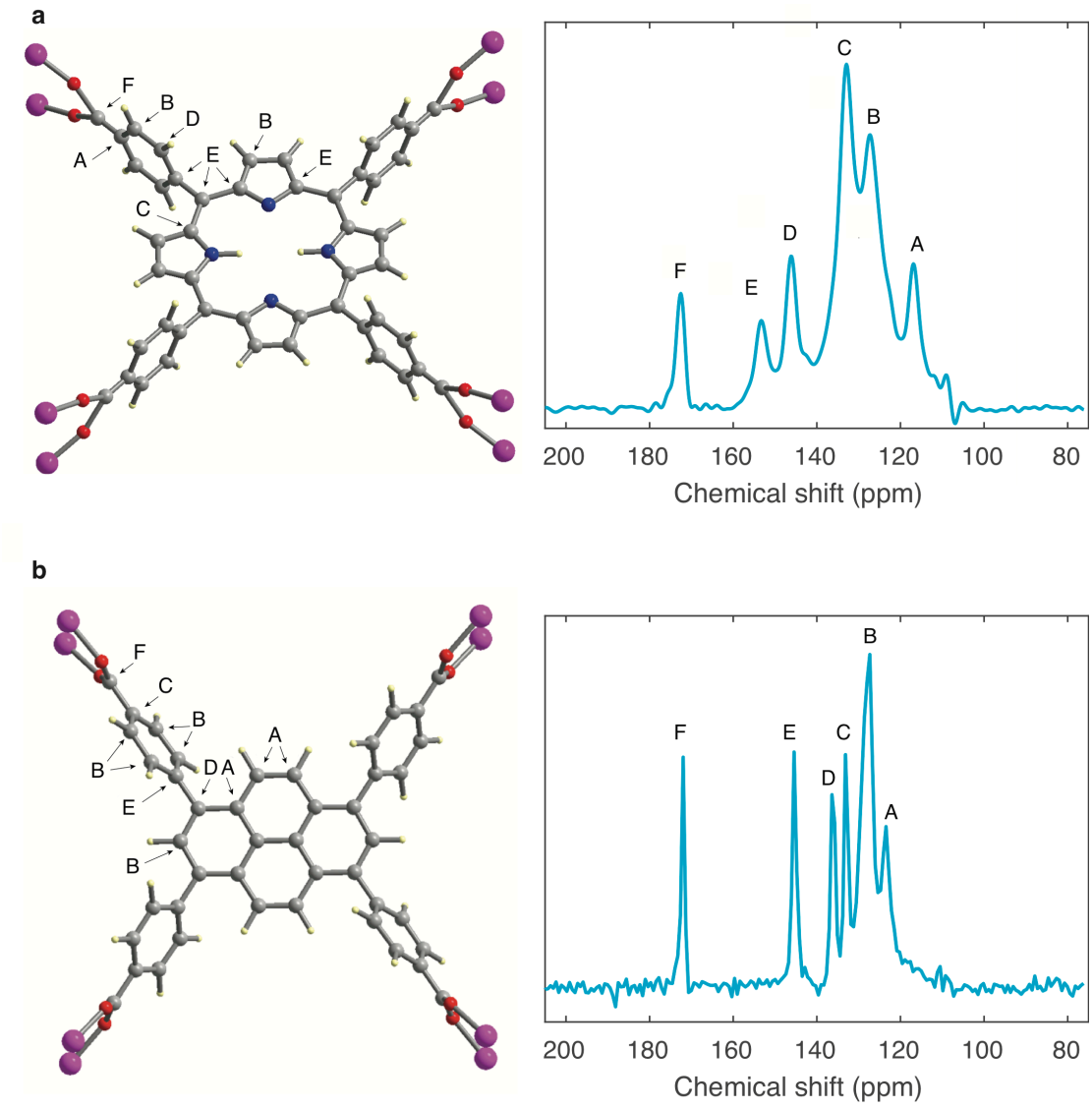

Extended Data Figure 8 | NMR spectra. ^{13}C CP-MAS spectrum of **a**, **Al-PMOF** and **b**, **Al-PyrMOF** recorded at 9.39 T with sample spinning at 8 kHz, the contact time for the CP experiment was 2 ms. The alphabets give chemical shift assignment to experimental spectrum.

MOF	Adsorbaphore Binding Energy (kcal/mol)		
	CO_2	H_2O	N_2
Al-PMOF	-12.6	-10.4	-7.9
Al-PyrMOF	-10.2	-8.7	-7.5

Extended Data Table 1 | DFT binding energies of gas particles in the adsorbaphore pocket of each MOF synthesized in this work

Metal species	*a* (Å)	*b* (Å)	**c (Å)**
Al(III)	15.84	30.33	**6.65**
Fe(III)	15.96	30.47	**6.83**
Ga(III)	15.97	30.56	**6.77**
In(III)	16.23	30.88	**7.27**
Sc(III)	16.12	30.70	**7.34**
Y(III)	16.43	30.72	**7.70**

Extended Data Table 2 | DFT optimized cell parameters of hypothetical MOFs

The MOFs are built with the **frz** topology and organic linker #67 (m8o67) and various trivalent metal species. The c-axis corresponds to the spacing between aromatic rings in the adsorbaphore.